Tilted Fiber Bragg Grating Inscription in Boron Co-Doped Photosensitive Optical Fiber Using 266 nm Solid State Laser Pulses

Xuehao Hu, Yingying Liu, Jie Jiang, Wenwei Lin, Hang Qu, and Christophe Caucheteur

***Abstract*—In the last decade, tilted fiber Bragg gratings (TFBGs) have received a lot of research attention due to their unique ability for detection of bending and surrounding refractive index (SRI). Meanwhile, fabrication of TFBGs normally requires fiber pre-hydrogenation and expensive laser systems, such as excimer laser at 193 nm or femtosecond lasers. In this work, we report the first TFBG inscriptions in Boron co-doping fibers (PS1250/1500, FIBERCORE) using low cost 266 nm solid state pulsed laser and scanning phase mask lithography technique. By using this inscription setup, gratings with tilt angles from 2° to 10° are fabricated. Influences (pulse repetition rate and scanning speed) on the grating quality and spectral performances are discussed. Furthermore, evolution of spectra during the inscription of the 10° TFBG is illustrated showing uniform growths of both the core and cladding modes. In addition to the TFBG fabrication, temperature, bending and SRI measurement are conducted. Because the core mode is restricted to propagate in the fiber core, TFBGs could automatically provide temperature compensation. The ease of TFBG fabrication and the capability of intrinsic temperature self-compensation pave the way to their potentially promising applications in curvature and refractometric measurement.**

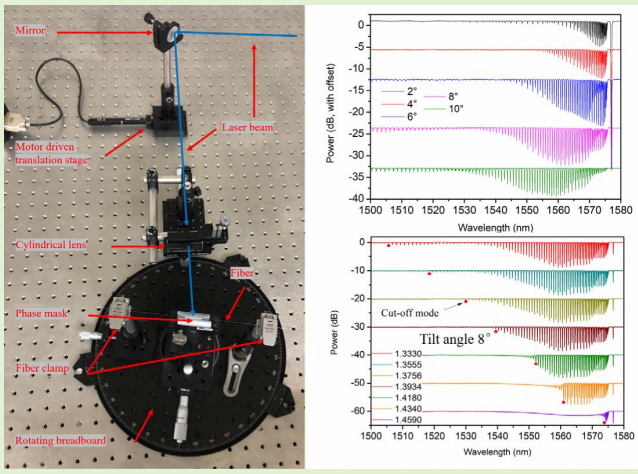

***Index Terms*—Boron co-doping fiber, tilted fiber Bragg grating, phase mask, solid state laser.**

I. Introduction

NOWADAYS, fiber Bragg gratings (FBGs) constitute important components in a variety of fiber-optic sensing systems for detection of e.g., temperature and strain. Advantages of fiber-optic sensors include compactness, immunity to EM interferences, resistance to corrosion, fast response and capacity of multi-parameter and quasi-distributed sensing [1]–[3]. Though FBGs are normally fabricated in silica optical fibers, they are also inscribed in polymer optical fibers (POFs) for sensing applications [4], [5]. Compared to traditional FBGs, long period fiber gratings (LPFGs) [6]–[8] and tilted fiber Bragg gratings (TFBGs) [9] are considered more advantageous for detection of bending and surrounding refractive index (SRI) due to their ability to excite cladding mode resonance which is the result from the coupling between core mode and cladding modes. However, for bending and SRI measurements, temperature cross-sensitivity normally is a problem that is difficult to solve for LPFGs. In contrast, TFBGs could automatically provide temperature compensation, since the core mode, which is restricted to propagate in the core, is immune to SRI. Moreover, compared to LPFGs, narrower resonances of TFBGs can induce higher wavelength measurement accuracy.

FBGs are fabricated by periodically modulating the refractive index in the core along the fiber axis, while TFBGs are inscribed with a slight tilt angle with respect to the fiber

Manuscript received November 19, 2021; revised December 17, 2021; accepted December 17, 2021. Date of publication December 21, 2021; date of current version January 31, 2022. This work was supported in part by the 2020 Li Ka Shing Foundation Cross-Disciplinary Research Grant 2020LKSFG01B and Grant 2020LKSFG14B, in part by the Specialized Project Fund in Science and Technology of Guangdong Province under Grant 2019ST135 and Grant 2019ST096, in part by the Special Projects in Key Fields of Colleges and Universities in Guangdong Province under Grant 2020ZDZX3035 and Grant 2020ZDZX3037, and in part by The Start-up Fund from Shantou University under Grant NTF19023 and Grant NTF18016. The associate editor coordinating the review of this article and approving it for publication was Prof. Carlos Marques. *(Corresponding author: Xuehao Hu.)*

Xuehao Hu, Yingying Liu, Jie Jiang, Wenwei Lin, and Hang Qu are with the Research Center for Advanced Optics and Photoelectronics, Department of Physics, College of Science, Shantou University, Shantou, Guangdong 515063, China, and also with the Key Laboratory of Intelligent Manufacturing Technology of MOE, Shantou University, Shantou, Guangdong 515063, China (e-mail: xhhu3@stu.edu.cn).

Christophe Caucheteur is with the Department of Electromagnetism and Telecommunication, University of Mons, 7000 Mons, Belgium.

Digital Object Identifier 10.1109/JSEN.2021.3137249

axis, respectively. To achieve this, the photosensitivity in silica optical fibers is of great importance. The photosensitivity of standard germanium-doped silica optical fibers (such as CORNING, SMF-28) is due to the Ge-Si wrong bond, and with UV irradiation, a creation of new defect is generated with refractive index change [10]. However, the photosensitivity of this standard fiber is relatively low for UV irradiation and it is not sufficient for inscriptions of high quality FBGs or TFBGs. Thus, researchers have made considerable efforts to improve the photosensitivity of germanosilica fibers by using hydrogen loading (hydrogenation) [11]–[13], flame brushing [14], 193 nm ArF excimer laser irradiation [12], [13], [15], [16], femtosecond laser pulses [13], [17], [18] or boron co-doping [19], [20]. However, hydrogenation and flame brushing need extra pre-treatment for photosensitivity enhancement, and 193 nm excimer lasers and femtosecond lasers are very expensive. Compared to these three methods, commercialized Boron co-doping fibers with UV lasers (∼250 nm), such as 266 nm solid state pulsed laser, can be used without any pre-treatment for both FBG and TFBG inscriptions due to extremely high photosensitivity, which improves the convenience and reduces the cost for TFBG fabrication.

Similar to FBGs, TFBGs are generally inscribed by interferometric or phase mask technique. For the former technique, an interferometer is used to split the laser beam into two parts and then recombine the two beams to generate an interference pattern [21]. This approach features advantages of high flexibility with respect to variations of grating periods and tilt angles. In contrary, for mass grating production with an identical grating period, phase mask technique is preferable. In this technique, the fiber is positioned within the interference pattern generated by a diffractive phase mask. The tilt angle is adjusted by keeping the fiber and phase mask perpendicular to the incident laser beam, while slightly rotating the phase mask around the axis of the laser beam; however, the diffracted beams from the rotated phase mask could distort the interference pattern inside the fiber [22], [23]. To solve this problem, Albert *et al.* proposed to rotate the phase mask and the fiber at the same time, since it provides a flatter fringe pattern inside the fiber [9], [24]. Also, in 2021 Wen *et al.* successfully manufactured TFBGs in Boron co-doping fibers (PS1250/1500, FIBERCORE) using the same inscription technique using a KrF excimer laser emitting at 248 nm [20]. A 10° TFBG was obtained in 6 minutes with the maximal amplitude of cladding modes to be ∼1.5 dB, which is not large enough for SRI sensing. Moreover, the 248 nm excimer laser is not cost-effective, similar as the 193 nm one. Besides, in 2014 Hu *et al.* reported the first TFBGs in trans-4-stilbenemethanol-doped photosensitive step-index poly(methyl methacrylate) (PMMA) POFs with tilt angles up to 4.5° [25].

In this work, to the best of our knowledge, we demonstrate the first TFBG inscriptions in Boron co-doping fibers (PS1250/1500, FIBERCORE) using the low cost 266 nm solid state pulsed laser and phase mask technique. First, gratings with tilt angles from 2° to 10° are inscribed with ∼3.2 mJ pulse energy and adapted pulse repetition rate from 25 Hz to 35 Hz. Then, the performance of the TFBG inscriptions with tilt angles of 2° and 8°, respectively, is discussed with respect to pulse repetition rate and scanning speed. Afterwards, dynamic spectra during the inscription of the 10° TFBG are recorded, showing that both the core and cladding modes in the transmitted amplitude spectra grow uniformly as a function of inscription time with a growth rate of 0.0076 dB/min and 0.17 dB/min, respectively, by linear regression.

Then, sensing applications based on TFBGs are conducted. Based on the 8° TFBG, the temperature sensitivities of the core mode at ∼1576.3 nm and the cladding mode at ∼1561.3 nm are very similar, which are 0.0083 ± 0.0002 nm/°C and 0.0085 ± 0.0001 nm/°C, respectively, so that the temperature cross-sensitivity of other sensing modalities, such as SRI and bending, can be eliminated by considering relative wavelength shifts instead of absolute wavelength measurements. The bending measurement is conducted with the 4° TFBG by monitoring the amplitude and the wavelength shift of the cladding mode at ∼1572.9 nm showing a sensitivity of 0.94 ± 0.03 dB/m^{-1} and −0.0163 ± 0.0004 nm/m^{-1}, respectively. Finally, the SRI measurements are carried out by monitoring the cut-off cladding mode of the 8° TFBG with a large SRI range from 1.3330 to 1.4590 showing a sensitivity of 543 ± 5 nm/RIU (refractive index unit). Besides, with a small SRI range from 1.3850 to 1.3854, the evolution of the cut-off mode at ∼1535.5 nm is recorded with a sensitivity of (5.8 ± 0.7) × 10^2 dB/RIU and (6.0 ± 0.4) × 10^2 nm/RIU, respectively.

II. Principle and Experimental Set-Up

A. Principle of TFBG

TFBGs belong to the short period (∼500 nm) grating family with a refractive index modulation direction slightly angled with respect to the optical fiber axis [9], [24], [25]. TFBGs have two mode-coupling mechanisms: self-backward coupling of the core mode and backward couplings between the core mode and numerous cladding modes [26]. The former generates Bragg mode or core mode similarly as FBGs, as expressed by

$$\lambda_{Bragg} = 2n_{eff,core}\Lambda_G \tag{1}$$

where $n_{eff,core}$ denotes the core effective refractive index, and Λ_G represents the grating period along the fiber axis.

For the latter coupling, TFBGs enable light to propagate in the cladding with different angles showing corresponding effective refractive indices of cladding modes $n_{eff,clad}$. Thus, wavelength of the cladding mode resonance is in one-to-one correspondence with its effective refractive index. This relationship is expressed by a phase-matching condition:

$$\lambda^i_{clad} = (n_{eff,core} + n^i_{eff,clad})\Lambda_G \tag{2}$$

where the superscript i denotes the mode number.

B. TFBG Fabrication and Experimental Set-Up

The 266 nm solid state pulsed laser (DPS-266-Q, Changchun New Industries Optoelectronics Tech. Co., Ltd) has a pulse width of ∼6 ns, a circle beam diameter of ∼2.5 mm and a beam divergence angle of ∼1 mrad at the laser output. The phase mask optimized at 266 nm positioned closely in front of the fiber has a pitch Λ_M of 1090 nm with a corresponding Λ_G of 545 nm, as in the case of pure two-beam

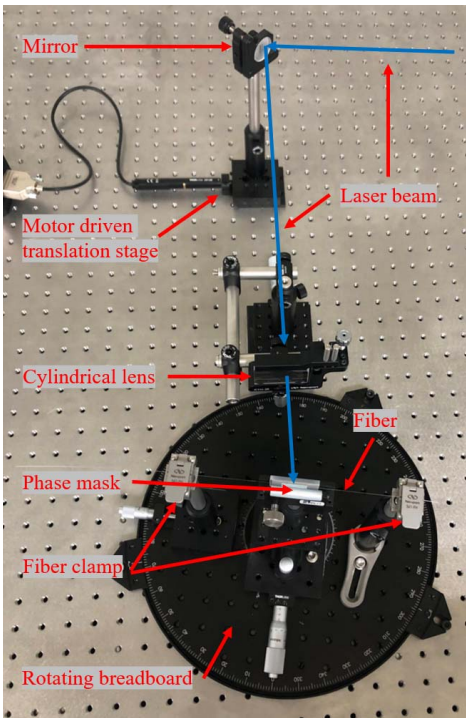

Fig. 1. Experimental set-up for TFBG inscription using 266 nm solid state laser pulses.

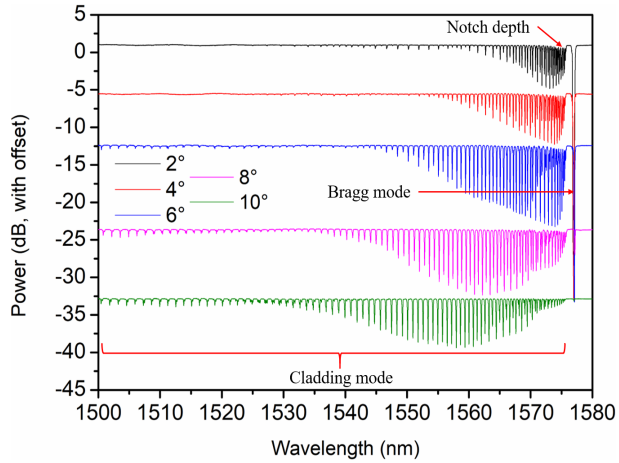

Fig. 2. TFBG transmitted spectra versus different tilt angles with adapted pulse repetition rate (2° / 25 Hz, 4° / 25 Hz, 6° / 35 Hz, 8° / 35 Hz, 10° / 35 Hz) and a constant scanning speed of 0.005 mm/s.

interference pattern, Λ_G is still given by Λ_M /2. Thus, TFBGs fabricated with different tilt angles are expected to have their Bragg resonances positioned at the same wavelength [27]. The experimental inscription set-up is illustrated in Fig. 1. The beam emitted from the solid state laser was firstly reflected by a mirror mounted on a motor driven translation stage. Then, a cylindrical lens with a focal length of 10 cm was used to focus the circle laser beam (∼4 mm in diameter) to ∼100 μm width along the fiber core for power density enhancement. The focused beam (4 mm long, 100 μm wide) scanned 12 mm to induce a 16-mm-long grating. Both the fiber and the phase mask were integrated on a rotating breadboard, so that they could be rotated by an identical angle. Due to the long Rayleigh length for such focal length, almost uniform power density was obtained during beam scanning without turning the cylindrical lens to adapt the rotation angle of the rotating breadboard (RBB300A/M, Thorlabs). The real-time spectrum recording relied on a grating interrogator (FS22SI, HBM Fiber Sensing) with a wavelength resolution of 1 pm and a scanning rate of 1 Hz.

III. Experimental Results and Discussions

A. TFBGs of Different Tilt Angles With Adapted Parameters

The tilt angle of TFBGs is a key factor to determine the resonance range of cladding modes corresponding to the measuring range of SRIs. In this experiment, TFBGs with tilt angles from 2° to 10° with a 2° interval were inscribed by optimizing the pulse repetition rate (20 Hz-40 Hz) at a constant scanning speed of 0.005 mm/s. The optimal repetition rates for 2° and 4° TFBGs are 25 Hz, while the counterparts for 6°, 8° and 10° TFBGs increase to 35 Hz. The transmitted amplitude spectra are shown in Fig. 2. Compared to variations of the repetition rate and the scanning speed, the shift of the pulse energy is limited, as it is 3.2 mJ at 20 Hz, and it gradually increases by ∼8% at 40 Hz. Thus, the influence of pulse energy could be neglected in this work. Fig. 2 shows that the insertion loss of the Bragg mode decreases from 27.90 dB to 0.33 dB as the TFBG tilt angle increases from 2° to 10°. Meanwhile, the central wavelength of the Bragg mode is almost constant at ∼1577 nm.

For cladding modes with increasing tilt angles, the maximal amplitude of the resonance is found to be 10.47 dB for the 6° TFBG and then decreases to 6.53 dB for the 10° TFBG, which agrees with the fact that the coupling efficiency of TFBG decreases with increasing tilt angles [26]. To improve the amplitude of the cladding mode for the 10° TFBG or to increase the tilt angle, generally much higher pulse energy or repetition rate is required; however, due to high risk of fiber breakage [28], 10° is the largest tilt angle implemented in this work. Besides, with increasing tilt angles, the spectral range of the cladding modes increases accordingly. Thus, TFBGs with a larger tilt angle can be applied to a smaller SRI measurement according to Equation (2). From 6°, the spectral range of the cladding modes is over 75 nm, though amplitude of the cladding mode is only ∼0.5 dB in the wavelength range under 1544.83 nm. Besides, laser irradiation-induced out-of-band insertion losses for different tilt angles were investigated by comparing the post-inscription spectra to the pre-inscription ones, showing very low insertion losses (maximal value: ∼ −0.1 dB for the 2° TFBG). Furthermore, the upper envelopes of these spectra are very smooth (maximal notch depth: ∼ −0.6 dB for the 6° TFBG). More detailed data are illustrated in Table I.

B. 2° TFBG Inscriptions

Fig. 3 presents the 2° TFBG inscriptions with respect to different pulse repetition rates and scanning speeds. It is shown that for a constant scanning rate of 0.01 mm/s, the maximal

TABLE I
TRANSMITTED SPECTRAL PARAMETERS FOR TFBGS OF VARIOUS TILT ANGLES

Tilt angle (°)	Pulse repetition rate (Hz)	Insertion loss of core mode (dB)	Wavelength of core mode (nm)	Maximal amplitude of cladding mode (dB)	Range of cladding mode resonance (nm)	Out-of-band insertion loss (dB)	Notch depth (dB)
2	25	27.90	1576.97	5.66	48.5	−0.103	−0.49
4	25	27.33	1576.98	6.51	50.6	−0.084	−0.54
6	35	20.86	1577.09	10.47	>75.0	−0.069	−0.62
8	35	3.29	1577.18	8.74	>75.0	−0.067	−0.42
10	35	0.33	1577.02	6.53	>75.0	−0.041	−0.06

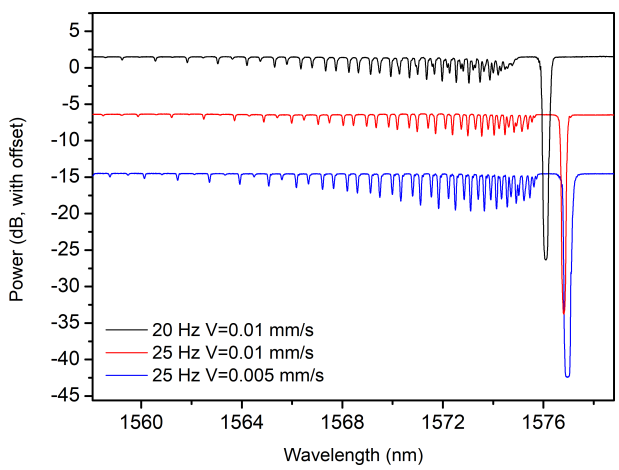

Fig. 3. 2° TFBG inscriptions with different parameters (20 Hz / 0.01 mm/s, 25 Hz / 0.01 mm/s, 25 Hz / 0.005 mm/s).

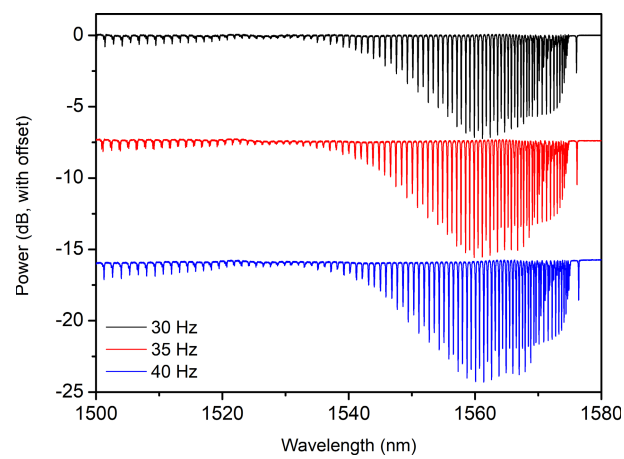

Fig. 4. 8° TFBG inscriptions with different pulse repetition rates (20 Hz, 35 Hz, 40 Hz) and a constant scanning speed of 0.005 mm/s.

cladding mode amplitude almost remains constant, as the repetition rate increases from 20 Hz to 25 Hz, suggesting that the repetition rate may not be a dominant factor for this TFBG improvement. Thus, the scanning speed was decreased to 0.005 mm/s, showing an almost doubled maximal cladding mode amplitude.

C. 8° TFBG Inscriptions

Fig. 4 presents the 8° TFBG inscriptions with a constant scanning speed of 0.005 mm/s; however, the pulse repetition rates are variable from 30 Hz to 40 Hz. It appears that the maximal cladding mode amplitude increases by 13.1% from 30 Hz to 35 Hz, while it increases by only 2.3% from 35 Hz to 40 Hz. However, the higher repetition rate increases the possibility of the fiber breakage due to accumulated heat [28]. Thus, the pulse repetition rate of 35 Hz is considered the most appropriate for the 8° TFBG inscription.

D. Dynamic Recording of the Transmitted Spectra During Inscription

Though TFBGs had been inscribed with different parameters, i.e., different tilt angles, pulse repetition rates and scanning speeds, both the core and cladding mode in the transmitted spectra of these TFBGs grow uniformly. Taking the 10° TFBG inscribed with a pulse repetition rate of 35 Hz and a scanning speed of 0.005 mm/s for example, as depicted in Fig. 5, the growth rates of their insertion losses (core mode and cladding mode with maximal amplitude) are 0.0076 ± 0.0003 dB/min and 0.17 ± 0.01 dB/min, respectively, by linear regressions, as shown in Fig.6.

E. TFBG Temperature Measurement

For the 8° TFBG inscribed with a pulse repetition rate of 40 Hz and a scanning speed of 0.005 mm/s, the temperature characterization was implemented between 20°C to 40°C with a step of 4°C. After the stabilization the spectra were recorded. Fig. 7 shows the linear fits of the central wavelength evolutions of the core mode at ∼1576.3 nm and the cladding mode at ∼1561.3 nm in terms of temperature, whose sensitivities are 0.0083 ± 0.0002 nm/°C and 0.0085 ± 0.0001 nm/°C, respectively. Thanks to the very similar sensitivities between the core mode and the cladding mode, the temperature cross-sensitivity of other sensing modalities, such as SRI and bending, can be eliminated by considering relative wavelength shifts instead of absolute wavelength measurements. This phenomenon is similar to the case reported in the previous work [9].

F. TFBG Bending Measurement

The bending experimental set-up is similar to the work [29]. Both sides of the 4° TFBG (repetition rate 25 Hz, scanning speed 0.005 mm/s) used in this measurement were fixed on two translation stages. The bending curvature was varied by adjusting the distance between the two sides, and the

TABLE II
PERFORMANCE COMPARISON OF BENDING SENSORS WITH DIFFERENT PRINCIPLES

Sensor structure	Sensing principle	Curvature sensitivity	Measurement range	Fabrication cost	Reproducibility and stability	Temperature cross-sensitivity	Reference
SMF-MMF-2CF-MMF-SMF	Modal interference	12.984 nm/m^{-1}	−1.2-−0.19 m^{-1}	Moderate	Low	0.069 nm/° C Not compensable	[31]
SMF-Offset SMF-SMF	Modal interference	−22.947 nm/m^{-1}	0.35312-2.8127 m^{-1}	Moderate	Low	77.6 pm/° C Not compensable	[32]
SMF-PCF-SMF	Modal interference	4.451 nm/m^{-1}	0-2.14 m^{-1}	Moderate	Low	7.78 pm/° C Not compensable	[33]
Inscribed FBGs in two core HEF	FBG	−16.9 pm/m^{-1} 33.3 pm/m^{-1}	0-4.759 m^{-1}	Moderate	Moderate	5.7 pm/°C 5.8 pm/°C Compensable	[34]
Offset SMF-LPFG in SMF	Mach-Zehnder interference and LPFG	−7.903 nm/m^{-1} 1.003 nm/m^{-1}	0.5-2.05 m^{-1}	Moderate	Low	58 pm/°C 49 pm/°C Compensable	[35]
Inscribed TFBG in SMF	TFBG	0.94 dB/m^{-1} −0.0163 nm/m^{-1}	1.68-4.79 m^{-1}	Low	High	0.0083 nm/°C 0.0085 nm/°C Compensable	This work

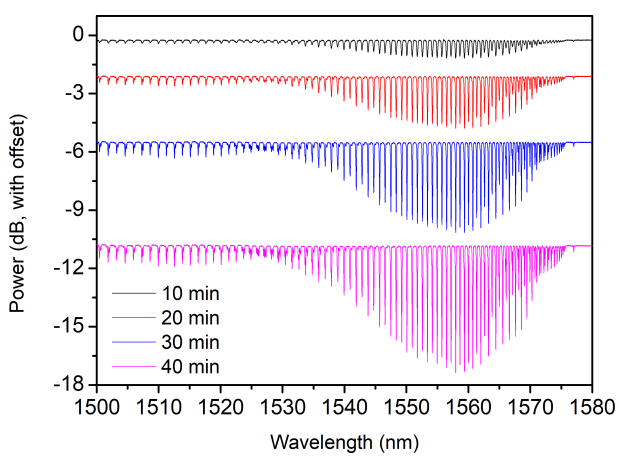

Fig. 5. Growth of the 10° TFBG transmitted spectrum with a pulse repetition rate of 35 Hz and a scanning speed of 0.005 mm/s.

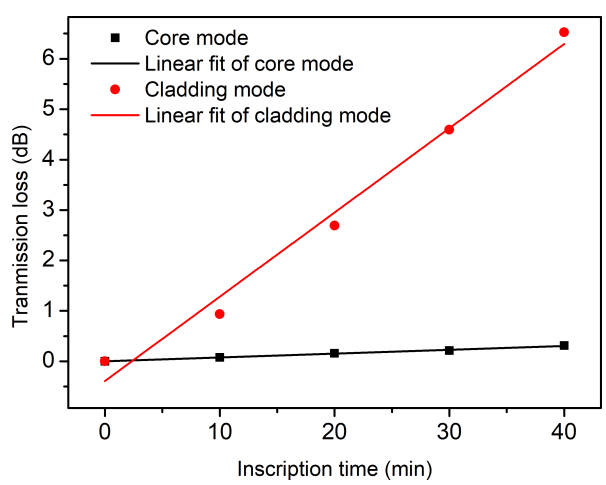

Fig. 6. Dynamic recording of the insertion losses of the core and the cladding (maximal amplitude) mode during inscription for the 10° TFBG with a pulse repetition rate of 35 Hz and a scanning speed of 0.005 mm/s.

approximate calculation of the curvature value can be found in the work [30]. The bending direction was optimized to obtain the highest bending sensitivity. Fig. 8 demonstrates

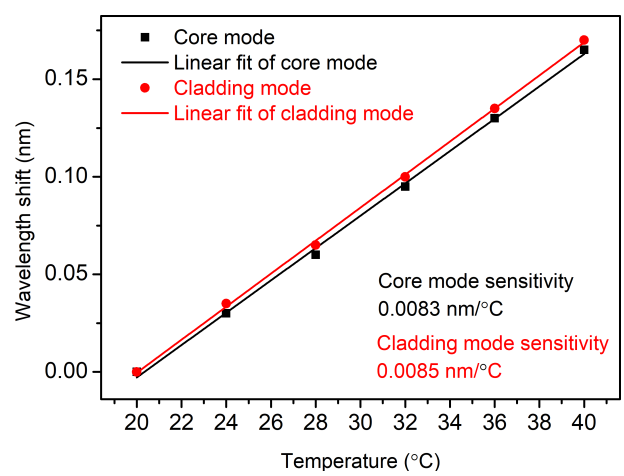

Fig. 7. Linear fits of the central wavelength evolutions of the core mode at ∼1576.3 nm and the cladding mode at ∼1561.3 nm versus temperature for the 8° TFBG.

the spectral evolution as a function of curvature including both the cladding mode and the core mode. It is found that the core mode at ∼1576.0 nm is stable during the experiment, while the cladding mode at ∼1572.9 nm is sensitive to the curvature. Consequently, the evolutions of the amplitude and the central wavelength of the cladding mode were linearly fitted with a sensitivity of 0.94 ± 0.03 dB/m^{-1} and −0.0163 ± 0.0004 nm/m^{-1}, respectively, as depicted in Fig. 9, which are higher than the results demonstrated in the Ref. [9]. The performance comparation between this bending sensor and other optical fiber-based sensors with different principles are presented in Table II.

G. TFBG Refractometric Measurement

The SRI measurement was conducted by immersing the sensing probe (8° TFBG: pulse repetition rate 35 Hz, scanning speed 0.005 mm/s) successively in glycerol/water solutions with different refractive indices covering a large SRI range from 1.3330 to 1.4590 (measured by an Abbe refractometer

TABLE III
PERFORMANCE COMPARISON OF REFRACTOMETRIC SENSORS WITH DIFFERENT PRINCIPLES

Sensor structure	Sensing principle	Curvature sensitivity	Measurement range	Fabrication cost	Reproducibility and stability	Temperature cross-sensitivity	Reference
SMF-etched MMF-SMF	Modal interference	286.2 nm/RIU	1.33-1.3775	Moderate	Low	- Not compensable	[36]
SMF-Offset tapered SMF-SMF	Modal interference	78.7 nm/RIU	1.333-1.374	Moderate	Low	- Not compensable	[37]
SMF-TCF-SMF	Modal interference	135.5 nm/RIU	1.3346-1.3899	Moderate	Moderate	0.015 nm/° C Not compensable	[38]
Etched multicore fiber	FBG	42.83 nm/ RIU	~1.435	Moderate	Moderate	9.89 pm/°C Compensable	[39]
Etched DCF	LPFG	~420 nm/RIU	~1.34	Moderate	Moderate	- Not compensable	[7]
Inscribed TFBG in SMF	TFBG	~580 dB/RIU ~600 nm/RIU	1.3850-1.3854	Low	High	0.0083 nm/°C 0.0085 nm/°C Compensable	This work

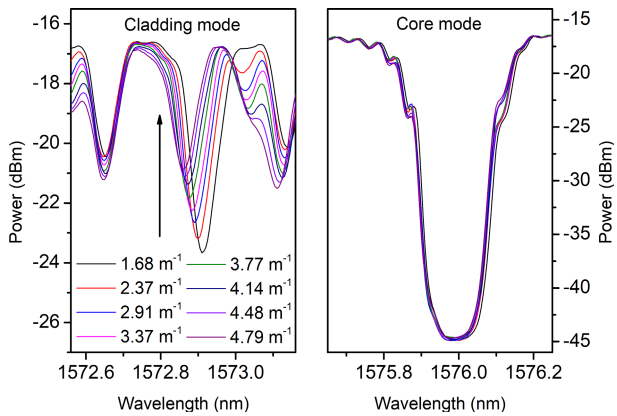

Fig. 8. Transmitted amplitude spectrum evolutions of the selected cladding mode at ~1572.9 nm and the core mode at ~1576.0 nm as a function of bending curvature for the 4° TFBG.

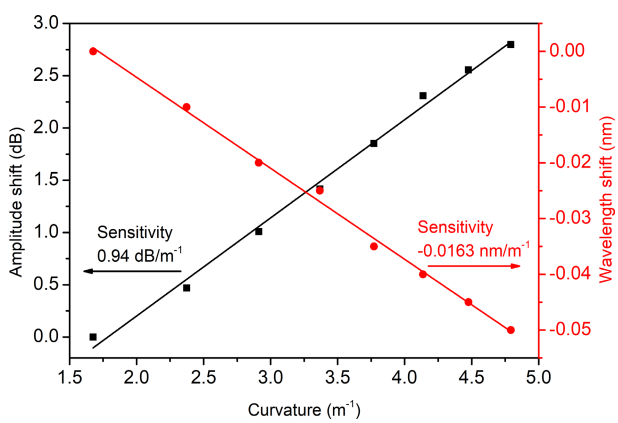

Fig. 9. Linear fits of the amplitude and the central wavelength evolutions of the cladding mode at ~1572.9 nm as a function of bending curvature for the 4° TFBG.

with an accuracy of 10^{-4}). Transmission spectra are presented in Fig. 10. It is found that the cladding mode resonances start to vanish from shorter wavelength to longer wavelength as the SRI value increases, which is similar to the case reported in

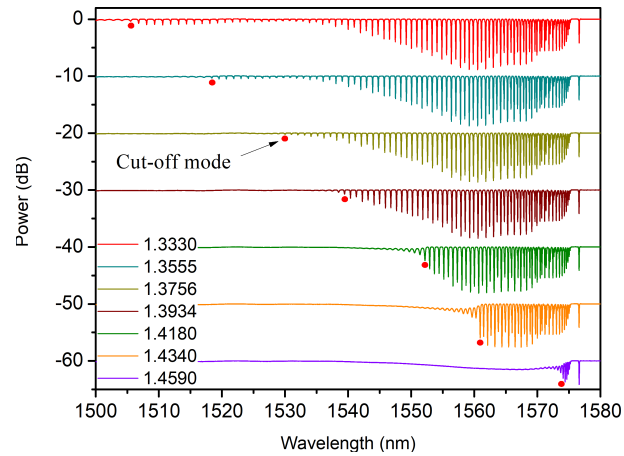

Fig. 10. Transmitted spectrum characterization of the 8° TFBG as a function of SRI.

the previous work [9], [24]. This behavior arises from the fact that when the SRI approaches the effective refractive index of a cladding mode (defined as cut-off mode), it is no longer reflected at the cladding-surrounding medium interface but becomes radiated. Consequently, a smooth line to the cut-off mode in the transmitted spectrum is demonstrated. The cut-off wavelength variations in terms of different SRIs are shown in Fig. 11, showing a sensitivity of 543 ± 5 nm/RIU.

In terms of small SRI measurement in the range from 1.3850 to 1.3854, the spectral evolutions of the cut-off mode and the core mode were recorded, as shown in Fig. 12. It is found that the core mode at ~1576.1 nm is stable during the experiment, while the cut-off mode at ~1535.5 nm is sensitive to the SRI. Thus, the evolutions of the amplitude and the central wavelength of the cut-off mode were linearly fitted showing a sensitivity of $(5.8 \pm 0.7) \times 10^2$ dB/RIU and $(6.0 \pm 0.4) \times 10^2$ nm/RIU, respectively, as depicted in Fig. 13, which is much higher than 38.67 nm/RIU in the range from 1.344 to 1.347 obtained from an 8° TFBG inscribed in a hydrogen-loaded standard single-mode germanosilicate optical fiber with a 193 nm ArF excimer laser [13]. In addition,

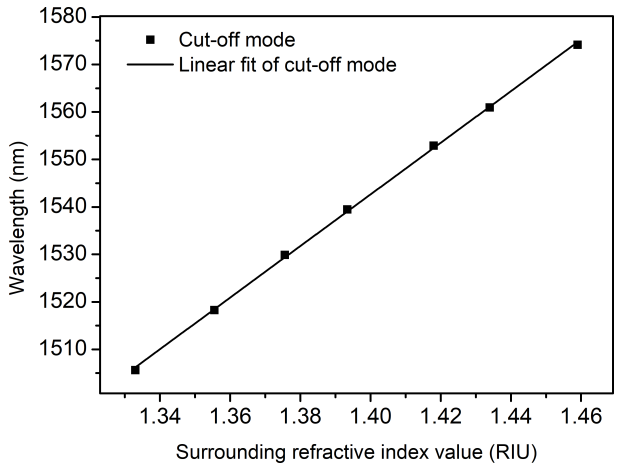

Fig. 11. Linear fit of cut-off cladding mode in transmitted spectrum versus SRI for the 8° TFBG.

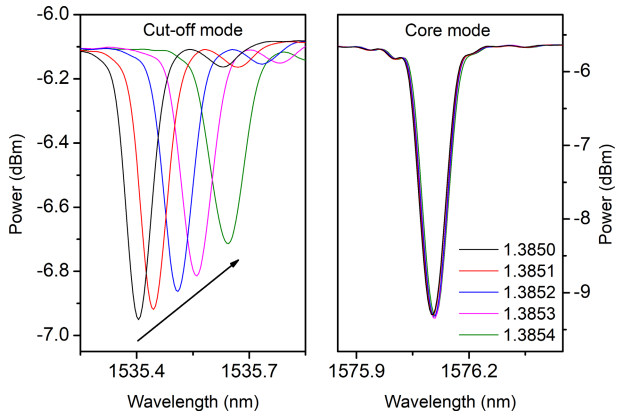

Fig. 12. Transmitted amplitude spectrum evolutions of the selected cladding mode at ∼1535.5 nm and the core mode at ∼1576.1 nm as a function of SRI for the 8° TFBG.

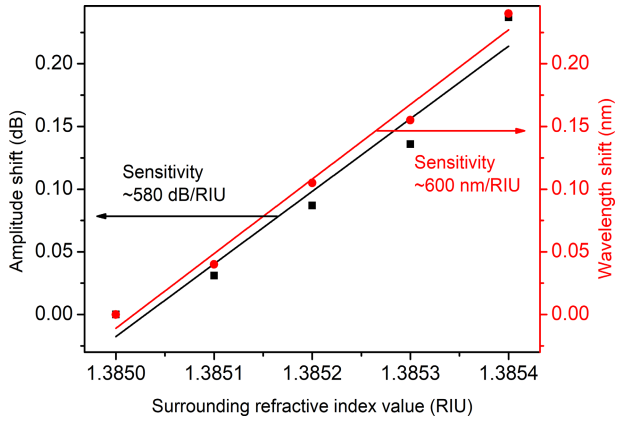

Fig. 13. Linear fits of the amplitude and the central wavelength evolutions of the cladding mode at ∼1535.5 nm as a function of SRI for the 8° TFBG.

the performance of this refractometric sensor is compared to other optical fiber-based sensors with different principles, as demonstrated in Table III.

IV. Conclusion

In summary, we demonstrated the first TFBG inscriptions in Boron co-doping fibers using a 266 nm UV laser together with scanning phase mask technique. The laser emits at 266 nm with a pulse width of ∼6 ns and a pulse energy of ∼3.2 mJ. By using this convenient and cost-effective inscription methodology, smooth gratings with tilt angles from 2° to 10° were fabricated. The maximal amplitude of the cladding mode resonance is equal to 10.47 dB for the 6° TFBG. Additionally, we found that compared to the pulse repetition rate, scanning speed plays a more important role on 2° TFBG inscription, while the pulse repetition rate of 35 Hz is the most appropriate for 8° TFBG inscription. Also, TFBGs grow uniformly as a function of time. It is worth mentioning that using the same inscription methodology, TFBGs are difficult to obtain in POFs, which could be due to the heat effect during the scanning process.

After TFBG inscriptions, their sensing applications were conducted. The similar temperature sensitivities of the core mode and the cladding mode ensure that the temperature cross-sensitivity for SRI and bending measurement can be eliminated by considering relative wavelength shifts. Also, the bending sensitivities are 0.94 dB/m^{-1} and −0.0163 nm/m^{-1}, respectively. In terms of SRI measurement, the evolution of the cut-off cladding mode was monitored showing sensitivities of 543 nm/RIU for a large SRI range from 1.3330 to 1.4590, and ∼580 dB/RIU / ∼600 nm/RIU for a small SRI range from 1.3850 to 1.3854. The ease of TFBG fabrication and the capability of intrinsic temperature self-compensation pave the way to their potentially promising applications in curvature and refractometric measurement.

References

[1] K. O. Hill, Y. Fujii, D. C. Johnson, and B. S. Kawasaki, "Photosensitivity in optical fiber waveguides: Application to reflection filter fabrication," *Appl. Phys. Lett.*, vol. 32, no. 10, pp. 647–649, 1978.

[2] A. Othonos, "Fiber Bragg gratings," *Rev. Sci. Instrum.*, vol. 68, no. 12, pp. 4309–4341, Dec. 1997.

[3] D. Kinet, P. Mégret, K. W. Goossen, L. Qiu, D. Heider, and C. Caucheteur, "Fiber Bragg grating sensors toward structural health monitoring in composite materials: Challenges and solutions," *Sensors*, vol. 14, no. 4, pp. 7394–7419, 2014.

[4] C. A. F. Marques *et al.*, "Fast Bragg grating inscription in PMMA polymer optical fibres: Impact of thermal pre-treatment of preforms," *Sensors*, vol. 17, no. 4, p. 891, 2017.

[5] A. G. Leal-Junior *et al.*, "Simultaneous measurement of axial strain, bending and torsion with a single fiber Bragg grating in CYTOP fiber," *J. Lightw. Technol.*, vol. 37, no. 3, pp. 971–980, Feb. 1, 2019.

[6] S. W. James and R. P. Tatam, "Optical fibre long-period grating sensors: Characteristics and application," *Meas. Sci. Technol.*, vol. 14, pp. R49–R61, Mar. 2003.

[7] F. Esposito, A. Srivastava, L. Sansone, M. Giordano, S. Campopiano, and A. Iadicicco, "Sensitivity enhancement in long period gratings by mode transition in uncoated double cladding fibers," *IEEE Sensors J.*, vol. 20, no. 1, pp. 234–241, Jan. 2020.

[8] F. Esposito *et al.*, "Label-free detection of vitamin D by optical biosensing based on long period fiber grating," *Sens. Actuators B, Chem.*, vol. 347, Nov. 2021, Art. no. 130637.

[9] J. Albert, L.-Y. Shao, and C. Caucheteur, "Tilted fiber Bragg grating sensors," *Laser Photon. Rev.*, vol. 7, no. 1, pp. 83–108, Feb. 2012.

[10] R. M. Atkins, V. Mizrahi, and T. Erdogan, "248 nm induced vacuum UV spectral changes in optical fibre preform cores: Support for a colour centre model of photosensitivity," *Electron. Lett.*, vol. 29, no. 4, pp. 385–387, Feb. 1993.

[11] P. J. Lemaire, R. M. Atkins, V. Mizrahi, and W. A. Reed, "High pressure H_2 loading as a technique for achieving ultrahigh UV photosensitivity and thermal sensitivity in GeO_2 doped optical fibres," *Electron. Lett.*, vol. 29, no. 13, pp. 1191–1193, Jun. 1993.

[12] C. Caucheteur, T. Guo, F. Liu, B.-O. Guan, and J. Albert, "Ultrasensitive plasmonic sensing in air using optical fibre spectral combs," *Nature Commun.*, vol. 7, no. 1, Nov. 2016, Art. no. 13371.

[13] N. S. Yazd, K. Chah, C. Caucheteur, and P. Megret, "Thermal regeneration of tilted Bragg gratings UV photo-inscribed in hydrogen-loaded standard optical fibers," *J. Lightw. Technol.*, vol. 39, no. 11, pp. 3582–3590, Jun. 1, 2021.
[14] F. Bilodeau *et al.*, "Photosensitization of optical fiber and silica-on-silicon/silica waveguides," *Opt. Lett.*, vol. 18, no. 12, pp. 953–955, Jun. 1993.
[15] J. Albert *et al.*, "Photosensitivity in Ge-doped silica optical waveguides and fibers with 193-nm light from an ArF excimer laser," *Opt. Lett.*, vol. 19, no. 6, pp. 387–389, Mar. 1994.
[16] J. Lao *et al.*, "*In situ* plasmonic optical fiber detection of the state of charge of supercapacitors for renewable energy storage," *Light, Sci. Appl.*, vol. 7, no. 1, Jul. 2018, Art. no. 34.
[17] J. He, B. Xu, X. Xu, C. Liao, and Y. Wang, "Review of femtosecond-laser-inscribed fiber Bragg gratings: Fabrication technologies and sensing applications," *Photonic Sensors*, vol. 11, no. 2, pp. 203–226, Apr. 2021.
[18] A. Ioannou, A. Theodosiou, C. Caucheteur, and K. Kalli, "Direct writing of plane-by-plane tilted fiber Bragg gratings using a femtosecond laser," *Opt. Lett.*, vol. 42, no. 24, pp. 5198–5201, 2017.
[19] D. L. Williams *et al.*, "Enhanced UV photosensitivity in boron codoped germanosilicate fibres," *Electron. Lett.*, vol. 29, no. 1, pp. 45–47, 1993.
[20] H.-Y. Wen, Y.-C. Hsu, S.-Y. Chen, and C.-C. Chiang, "The manufacturing process and spectral features of tilted fiber Bragg gratings," *Opt. Laser Technol.*, vol. 134, Feb. 2021, Art. no. 106615.
[21] K. Zhou, A. G. Simpson, L. Zhang, and I. Bennion, "Side detection of strong radiation-mode out-coupling from blazed FBGs in single-mode and multimode fibers," *IEEE Photon. Technol. Lett.*, vol. 15, no. 7, pp. 936–938, Jul. 2003.
[22] S. J. Mihailov *et al.*, "UV-induced polarisation-dependent loss (PDL) in tilted fibre Bragg gratings: Application of a PDL equaliser," *IEE Proc.-Optoelectron.*, vol. 149, no. 56, pp. 211–216, Oct. 2002.
[23] C. Caucheteur and P. Megret, "Demodulation technique for weakly tilted fiber Bragg grating refractometer," *IEEE Photon. Technol. Lett.*, vol. 17, no. 12, pp. 2703–2705, Dec. 2005.
[24] T. Guo, F. Liu, B.-O. Guan, and J. Albert, "Tilted fiber grating mechanical and biochemical sensors," *Opt. Laser Technol.*, vol. 78, pp. 19–33, Apr. 2016.
[25] X. Hu, C.-F. J. Pun, H.-Y. Tam, P. Mágret, and C. Caucheteur, "Tilted Bragg gratings in step-index polymer optical fiber," *Opt. Lett.*, vol. 39, no. 24, pp. 6835–6838, Dec. 2014.
[26] T. Erdogan and J. Sipe, "Tilted fiber phase gratings," *J. Opt. Soc. Amer. A, Opt. Image Sci.*, vol. 13, no. 2, pp. 296–313, 1996.
[27] N. Abdukerim, D. Grobnic, C. Hnatovsky, and S. J. Mihailov, "Through-the-coating writing of tilted fiber Bragg gratings with the phase mask technique," *Opt. Exp.*, vol. 27, no. 26, pp. 38259–38269, Dec. 2019.
[28] R. Oliveira, L. Bilro, and R. Nogueira, "Bragg gratings in a few mode microstructured polymer optical fiber in less than 30 seconds," *Opt. Exp.*, vol. 23, no. 8, pp. 10181–10187, 2015.
[29] Y. Zhao, L. Cai, and X.-G. Li, "Temperature-insensitive optical fiber curvature sensor based on SMF-MMF-TCSMF-MMF-SMF structure," *IEEE Trans. Instrum. Meas.*, vol. 66, no. 1, pp. 141–147, Jan. 2017.
[30] Y. Wang *et al.*, "Intensity measurement bend sensors based on periodically tapered soft glass fibers," *Opt. Lett.*, vol. 36, no. 4, pp. 558–560, 2011.
[31] S. Wang *et al.*, "Bending vector sensor based on the multimode-2-core-multimode fiber structure," *IEEE Photon. Technol. Lett.*, vol. 28, no. 19, pp. 2066–2069, Oct. 1, 2016.
[32] L. Mao, P. Lu, Z. Lao, D. Liu, and J. Zhang, "Highly sensitive curvature sensor based on single-mode fiber using core-offset splicing," *Opt. Laser Technol.*, vol. 57, pp. 39–43, Apr. 2014.
[33] H. Gong, H. Song, X. Li, J. Wang, and X. Dong, "An optical fiber curvature sensor based on photonic crystal fiber modal interferometer," *Sens. Actuators A, Phys.*, vol. 195, pp. 139–141, Jun. 2013.
[34] G. Mao *et al.*, "Fiber Bragg grating sensors in hollow single-and two-core eccentric fibers," *Opt. Exp.*, vol. 25, no. 1, pp. 144–150, Jan. 2017.
[35] S. Zhang, W. Zhang, P. Geng, and L. Wang, "A Mach–Zehnder interferometer constructed using lateral offset and a long period fiber grating for two-dimensional bending vector sensing," *J. Opt.*, vol. 16, no. 1, Nov. 2013, Art. no. 015501.
[36] Y. Zhao, L. Cai, X.-G. Li, F.-C. Meng, and Z. Zhao, "Investigation of the high sensitivity RI sensor based on SMS fiber structure," *Sens. Actuators A, Phys.*, vol. 205, pp. 186–190, Jan. 2014.
[37] Y. Zhao, X.-G. Li, and L. Cai, "A highly sensitive Mach–Zehnder interferometric refractive index sensor based on core-offset single mode fiber," *Sens. Actuators A, Phys.*, vol. 223, pp. 119–124, Mar. 2015.
[38] T.-H. Xia, A. P. Zhang, B. Gu, and J.-J. Zhu, "Fiber-optic refractive-index sensors based on transmissive and reflective thin-core fiber modal interferometers," *Opt. Commun.*, vol. 283, no. 10, pp. 2136–2139, 2010.
[39] W. Hu, C. Li, S. Cheng, F. Mumtaz, C. Du, and M. Yang, "Etched multicore fiber Bragg gratings for refractive index sensing with temperature in-line compensation," *OSA Continuum*, vol. 3, no. 4, pp. 1058–1067, Apr. 2020.

Xuehao Hu was born in China in 1981. He received the bachelor's degree in optical information science and technology and the master's degree in quantum optics from the Physics Department, Jilin University, China, in 2005 and 2008, respectively, and the Ph.D. degree in science of engineering and technology from the University of Mons, Belgium, in 2017. He is currently working as an Associate Professor with the College of Science, Shantou University, China. His research interest focuses on fiber Bragg gratings, tilted fiber Bragg gratings, polymer optical fiber sensors, surface plasmon resonance, and biosensors.

Yingying Liu received the B.Eng. degree in electronic information engineering from Henan Normal University, Xinxiang, China, in 2018. Now, she is working as a Research Assistant with Shantou University under the supervision of Xuehao Hu. Her research interests mainly focus on fiber Bragg gratings, tilted fiber Bragg gratings, surface plasmon resonance, and biosensors.

Jie Jiang works as a Research Assistant with Shantou University under the supervision of Xuehao Hu. His research interest mainly focuses on fiber Bragg gratings, tilted fiber Bragg gratings, and polymer optical fibers.

Wenwei Lin works as a Research Assistant with Shantou University under the supervision of Xuehao Hu. His research interests mainly focus on fiber Bragg gratings, tilted fiber Bragg gratings, surface Plasmon resonance, and biosensors.

Hang Qu received the B.Sc. and M.Sc. degrees in physics from Jilin University, China, in 2005 and 2007, respectively, and the Ph.D. degree in engineering physics from the Ecole Polytechnique de Montreal, Canada, in 2013. From 2014 to 2018, he worked as a Research Fellow with the Ecole Polytechnique de Montreal, where his research focused on fabrication of microstructured optical fibers and multifunctional and multimaterial fibers. Since 2018, he has been an Associate Professor with the College of Science, Shantou University. His current research interests include design and fabrication of microstructured optical fibers for sensing and telecommunications, design and fabrication of multifunctional/multimaterial fibers for wearable applications, and artificial skin sensors.

Christophe Caucheteur received the master's degree in electrical engineering and the Ph.D. degree in applied sciences from the Faculté Polytechnique de Mons, Belgium, in 2003 and 2007, respectively. He is currently a Senior Research Associate of the F.R.S.-FNRS with the University of Mons. He is also the Head of the Advanced Photonic Sensors ERC Unit. He is the coauthor of about 250 papers in international journals and conference proceedings. He is also coauthor of six international patent applications regarding the development of innovative fiber Bragg gratings sensors. He received a European Research Council Starting Grant for a research project focused on the development of innovative plasmonic biochemical optical fiber sensors.